HOSTED BY
ELSEVIER
Available online at www.sciencedirect.com
ScienceDirect
Soils and Foundations 63 (2023) 101401
SOILS AND FOUNDATIONS
www.elsevier.com/locate/sandf

Technical Paper

Axial capacity ageing trends of large diameter tubular piles driven in sand

D. Cathie [a], R. Jardine [b,*], R. Silvano [a], S. Kontoe [d,b], F. Schroeder [c]

[a] *Cathie Group, Belgium*
[b] *Department of Civil and Environmental Engineering, Imperial College London, UK*
[c] *Geotechnical Consulting Group LLP, London, UK*
[d] *University of Patras, Greece*

Received 2 May 2023; received in revised form 14 October 2023; accepted 31 October 2023
Available online 20 November 2023

Abstract

The paper examines dynamic pile test data from 25 high-quality offshore cases, where end-of-initial driving (EoID) and beginning-of-restrike (BoR) instrumented dynamic monitoring was undertaken on tubular piles driven in sands at well-characterised sites after known setup periods. The static resistances derived from signal matching by two independent specialist teams using different software are compared with CPT-based pile capacity calculations, providing the first axial capacity and setup dataset for large offshore piles driven in sand. Complementary re-analyses are made from three onshore/nearshore sites where dynamic and static testing was conducted on comparable piles. Open-ended tubular steel piles with 0.3–3.5 m diameters driven in (mainly dense) sands are all shown to develop marked setup, which is most active over the first 2–10 days. All piles show similar outcomes 20–30 days after installation. However, the larger diameter offshore piles' dynamic tests indicate no further setup after 30 days, while smaller diameter piles at onshore/nearshore sites continue to display further marked capacity growth. Comparisons of the axial shaft capacities inferred from signal matching with CPT-based design methods provides insights into the performance of the design methods. A trend for long-term pile shaft set-up to decrease with increasing diameter is identified and ascribed principally to the diameter-dependent constrained dilatancy that develops under axial loading at the pile-sand interface.
© 2023 Production and hosting by Elsevier B.V. on behalf of The Japanese Geotechnical Society. This is an open access article under the CC BY-NC-ND license (http://creativecommons.org/licenses/by-nc-nd/4.0/).

Keywords: Piles; Sand; Shaft capacity; Time effects; Pile driving

1. Introduction

Driven open-ended tubular steel piles support thousands of offshore and other structures and predicting their axial capacities reliably is central to ensuring safe and economical designs. Calibration against statistically significant pile test databases has been central to the development of CPT-based design methods for sands such as the ICP-05, UWA-05 and Unified methods; Jardine and Chow, 1996; Jardine et al., 2005; Lehane et al., 2005; Yang et al., 2017; Lehane et al., 2017, 2020). While it is well known that axial capacities grow with time in sand (Jardine et al., 2006; Gavin et al., 2015) design guidance does not yet cover conditions for ages greater than the ≈25-day mean applying to the ICP-05's database and the Unified database's ≈14-day median age. The CPT methods' application to offshore conditions may also be questioned because of their calibration database populations. Of the Unified database's 29 high-quality tests on open tubular steel (principally onshore) piles driven in sands, only one had an outside diameter $D > 0.81$ m. In contrast, axially loaded offshore piles may have diameters exceeding 3.5 m. Their groundwater salinity and temperatures also differ from most

* Corresponding author.
E-mail address: r.jardine@imperial.ac.uk (R. Jardine).

https://doi.org/10.1016/j.sandf.2023.101401
0038-0806/© 2023 Production and hosting by Elsevier B.V. on behalf of The Japanese Geotechnical Society.
This is an open access article under the CC BY-NC-ND license (http://creativecommons.org/licenses/by-nc-nd/4.0/).

Nomenclature

CPT Cone penetration test
CW CAPWAP wave equation signal matching program
CoV Coefficient of variation
DEM Discrete element method
Enthru Energy transmitted to the pile during a single blow
EoID, BoR End of Initial Drive, Beginning of Restrike
FEM Finite element method
IM IMPACT wave equation signal matching program
MQ Match quality
PAGE Pile Ageing Joint Industry Project
SRD Soil resistance during driving (axial resistance)
TTBH Trans-Tokyo Bay Highway project
WEAP GRLWEAP wave equation pile driving simulation program
A, B, C Fitting parameters for change in resistance with time (t) - equation (1)
D, OD Outside diameter
D_r, $D_{r,ave}$ Relative density, average relative density
d_{50} Seive size for 50% particles passing
G_{max} Small strain shear modulus
G Shear modulus
L Embedded pile length
q_t, $q_{t,ave}$ Cone resistance, average cone resistance
R_{total}, R_{shaft}, R_{toe} Static axial resistances (total, shaft component, toe component)
$R_{Static\text{-}comp}$, $R_{Static\text{-}tens}$ Static axial pile resistances measured in either compression or tension pile load tests
$R_{shaft,m}$, $R_{shaft,c}$ Measured and calculated axial shaft resistances
R_{EoID}, R_{BoR} Total static pile resistance (SRD) from signal matching at EoID or BoR
$R_{ICP\text{-}05}$, $R_{UNIFIED}$ Static axial pile resistances calculated by ICP-05, or UNIFIED methods
R_{IM}, R_{CW} Static axial pile resistances derived by IMPACT and CAPWAP signal matching
R_{CLA} Interface Centre-Line-Average roughness
S_{total}, S_{shaft}, S_{toe} Setup defined as ratio of axial resistance after setup at BoR (R_{BoR}) or static testing and axial resistance at EoID (R_{EoID}) for total, shaft and toe resistances
t_w Pile wall thickness
t Time in days since EoID
δ Interface shear angle
φ' Angle of shearing resistance
σ'_{rc} Pile shaft radial effective stress before loading
σ'_{rf} Pile shaft radial effective stress at failure
$\Delta\sigma'_{rd}$ Dilatant increase in local radial effective stress due to interface dilation including any effect of long-term corrosion-related ageing
ε_c Cavity strain
Δr Radial displacement at interface due to dilation, potentially boosted by ageing

onshore tests, and offshore driving procedures vary from typical onshore practice.

Static testing on offshore piles with diameters greater than 1 m has only proved feasible in exceptional circumstances (Barbosa et al., 2015). However, key insights may be gained at well-characterised sites if piles instrumented with strain gauges and accelerometers are monitored during driving and later re-strike tests. Signal matching analyses can then provide soil resistance-to-driving profiles for comparison with design capacities; see Overy (2007) or Jardine et al. (2015). The Pile Ageing (PAGE) Joint Industry Project (JIP) applied such analyses to generate a new dynamic test dataset for large offshore piles driven in sand. PAGE examined 25 high-quality paired offshore end-of-initial-drive (EoID) and beginning-of-restrike (BoR) cases, rigorously reviewing each pile's geotechnical profile, dynamic testing and driving records before applying consistent and systematic axial capacity and dynamic test analyses. The offshore cases were complemented by re-analyses of impact and monotonic static tests on open-ended steel piles at several onshore sites that facilitated comparisons between dynamic and static testing trends.

2. Earlier studies

Jardine et al. (2006) reported tests to failure on identical approximately 19 m long, 457 mm outer diameter (D) tubular steel piles driven at the well-characterised Dunkirk dense sand research site in northern France. While repeated tension loading was shown to damage capacity and give misleading ageing trends, first-time tension tests demonstrated the strong growth in shaft resistance over 235 days, with little apparent change in initial axial stiffness shown in Fig. 1. Jardine et al. (2006) postulated four potential mechanisms for the growth of shaft capacity:

- Local radial stresses rising through stress redistribution linked to creep weakening circumferential arching around the shafts.

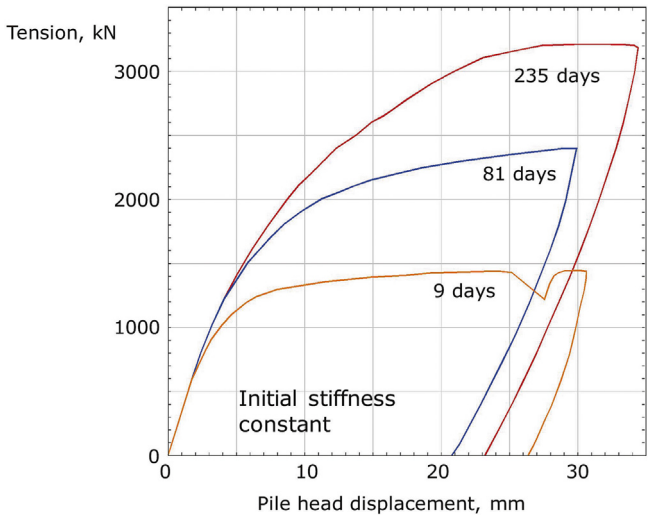

Fig. 1. First-time static tests on piles driven at Dunkirk, re-drawn from Jardine et al (2006) Note: $R_{shaft,m}$ and $R_{shaft,c}$ are the shaft resistances measured and calculated, respectively.

- Bonding of sand grains to shafts raising interface shear angles δ, from for example ≈29° to critical state $\varphi' \approx 32°$ and boosting capacity by 10–15%.
- Corrosion reactions raising local radial shaft effective stresses σ'_{rc} through cylindrical cavity expansion and increasing pile centreline shaft roughnesses R_{CLA} and interface shear δ angles as above.
- Enhanced interface dilation boosting σ'_r during loading to failure by increments $\Delta\sigma'_{rd}$, due to additional dilative radial displacements Δr developing at the shaft. Shear stiffness changes might also contribute, although the similar initial pile loading slopes shown in Fig. 1 indicate that such changes may not contribute significantly.

Rimoy et al. (2015) synthesised tests on similar piles driven in loose saturated sand at Larvik, Norway (Karlsrud et al., 2014) and dense unsaturated sand at Blessington, Ireland (Gavin et al., 2013) and noted similar trends between their aged shaft capacities, $\underline{R_{shaft,m}}$ and those calculated by with ICP-05, $\underline{R_{shaft,c}}$, as shown in Fig. 2. Axelsson (2000) and Gavin et al. (2013) reported mixed evidence from normal stress measurements regarding σ'_{rc} growth over time around closed-end piles and Rimoy et al. (2015) noted that 36 mm diameter stainless steel, closed-ended, model piles developed almost no capacity gains over extended durations in laboratory calibration-chamber experiments. However, Jardine (2020) reported independent FEM and DEM analyses that support the postulated creep-arching mechanism and argued that the mechanism could be more effective around larger piles.

Carroll et al. (2020) drove tens of 50–60 mm diameter, mild-steel and stainless/galvanised steel, open-ended, micro-piles at the same sites as the Fig. 2 tests. While stainless-steel micro-piles showed no tension capacity gain over 2 years after driving, corrodible mild steel micro-piles showed significant setup, although less than the earlier tests on larger piles, that levelled off within ≈1 year. They also noted marked increases in shaft roughness due to corrosion and sand grain adhesion.

One potential cause for scale dependency in ageing is the crushed sand 'crust' that adheres to both laboratory model

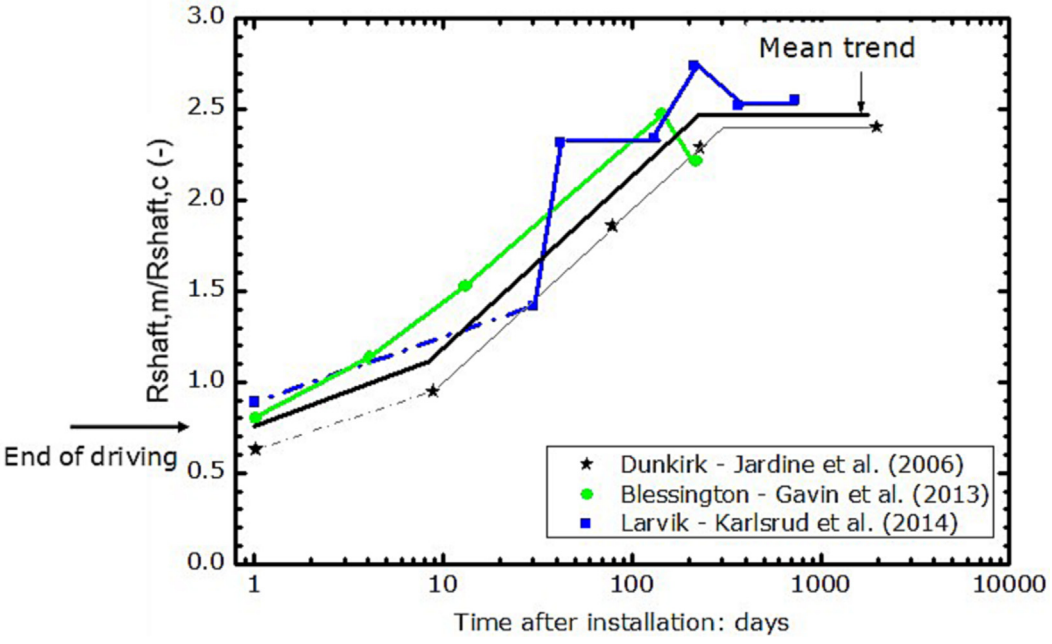

Fig. 2. Trends for growth in first-time shaft capacity with timeat three sites, tension capacities normalised by pile specific ICP-05 predictions(after Rimoy et al., 2015) Note: Setup determined from static tension and compression tests denoted as S-T and S-C, respectively, compared to EoID dynamic tests.

and field-driven piles. Extensive grain crushing occurs beneath pile tips and within an annular shear zone region around their shafts whose thickness depends on grain size and potentially pile wall thickness; Ho et al. (2011). The steel also corrodes slowly. Ohsaki (1982) studied how anoxic corrosion progressed with 126 steel driven piles over 2, 5 and 10-year periods of embedment at ten sand, gravel, silt and clay sites. The average steel loss rates found on plane surfaces amounted to ≈40 μm over the first two years, with rates slowing thereafter. While scattered, the rates did not vary markedly with soil type or groundwater conditions. Iron corrosion compounds gradually encrust the crushed sand zones found around steel shafts; Chow (1997), Ohsaki (1982), Kolk et al. (2005), Yang et al. (2010), Gavin et al. (2013) and Carroll et al. (2020).

Axelsson (2000) and Gavin et al. (2015) confirmed that enhanced interface dilation makes an important contribution to long-term setup on relatively small closed-end piles, although its influence is expected to reduce with increasing pile diameter; Jardine et al. (2005). In common with Chow (1997) and Rimoy et al. (2015), Axelsson (2000) reported that concrete driven piles show significant ageing gains that cannot be related to steel corrosion.

Jardine et al. (2015) employed dynamic stress-wave matching analyses for 2.1 m OD offshore jacket piles driven in very dense marine sands in the German North Sea to assess their capacities. CAPWAP signal matching was undertaken for EoID conditions; a BoR check performed 6 days later indicated 45%, short-term, shaft capacity growth that could not be reconciled with corrosion.

Cathie et al. (2022) collated further cases histories where open tubular steel piles, with D > 0.45 m, were tested dynamically or statically after known ageing periods; see Table 1. The overall trends plotted in Fig. 3, show dynamic (signal-matched) and static shaft capacities growing by 50% above their dynamic EoID shaft resistances within ten days and setup factors that exceed 2.0 after ≈100 days.

3. PAGE methodology

The PAGE project aimed to assess the ageing behaviour of large driven offshore piles through comprehensive dynamic testing. While static tests give more certain results, none have been reported on large offshore piles driven in sand. The scope for assessing compressive axial pile capacities by dynamic signal matching is discussed by Rausche et al. (1972); Rausche et al. (1985); Randolph (1993); Likins and Rausche (2004); Loukidis et al.,(2008) and many others, and is addressed in some pile design codes of practice (e.g. DGGT, 2013; EC7, 2004). Signal matching involves an inversion process that does not yield unique solutions, making the results user-dependent (Fellenius, 1988). Good practice for obtaining representative indications of static resistances involves undertaking at least two independent analyses by experienced professionals (DIN 18088-4, 2019; Likins et al., 1996).

Cathie et al. (2022) describe how PAGE adopted best-practice signal matching and axial capacity calculation procedures. Full geotechnical characterisation, pile design, installation and dynamic pile test datasets were obtained for each case. Signal matching was performed for selected locations by independent teams using the differently formulated CAPWAP (PDI, 2006) and IMPACT (Randolph, 2008) signal matching codes to address model uncertainty.

Wen et al. (2023) addressed the potential uncertainty in gauging static capacity trends from dynamic tests by correlating for PAGE dynamic stress-wave analyses and static tests on 762 mm diameter piles driven at the EURIPIDES dense sand research site (see Zuidberg and Vergobbi, 1996; Kolk et al., 2005). Broadly consistent shaft resistance trends were found over the first few days after driving. Additional broad confirmation was obtained for PAGE by considering piles tested at known ages after driving at the Horstwalde (Rücker et al., 2013) and Trans Tokyo Bay (Shioi et al., 1992; Sawai et al., 1996) sites.

3.1. Dynamic test dataset

Table 2 summarises the PAGE offshore dataset of 25 large diameter piles with outside diameters (D) from 1.3 m to 3.4 m, length to diameter ratios (L/D) of 8–53, and diameter to wall thickness (t_w) ratios (D/t_w) between 18 and 67. All were driven by hydraulic impact hammers; sufficient CPT and borehole data was available to enable reliable soil resistance to driving and static axial resistance calculations by the Alm and Hamre (2001), ICP-05 and Unified methods. The soil conditions at all sites were such that sand dominated layers are assessed as contributing at least 75% of the total shaft resistance. Table 2 provides the average cone tip resistances $q_{t,avg.}$ and mean relative densities, $D_{r,avg.}$ for each site, and shows a range of $q_{t,avg}$ from 21 to 62 MPa, and $D_{r,avg.}$ of 76–100%, indicating the dominance of medium dense to very dense sand sites in the PAGE dataset. One site, offshore Indonesia, had significant layers of clay and gravel, although a thick sand layer contributed most of the pile's shaft resistance.

Good quality dynamic data was available from EoID and BoR blows at each site to assess ageing (set-up) after periods between 8 h and 374 days after driving. CAPWAP signal matching analyses were performed for all 25 cases, and IMPACT check analyses for 12. The available evidence indicates that all piles drove without plugging. At 10 locations (including 7 from one project), the permanent pile displacements (sets) achieved at BoR fell below the 2.5 mm minimum indicated by PDI (2006) for shaft resistance mobilisation. To make best use of these tests' valuable information, a 'calibrated wave equation analysis' procedure, as employed by Battacharya et al. (2009) and Argiolas and Jardine (2017) in other offshore cases, was applied in GRLWEAP (PDI, 2010; Rausche et al., 2009) analyses of the BoR resistances of the 8 piles with the greatest (52–81 day) ages. Independent IMPACT analyses were performed to check the results. The reliability of the 'cali-

Table 1
Setup data from literature.

Project	Pile Ref.	D (m)	t_w [1] (mm)	D/ t_w (-)	L[2] (m)	L/D (m)-	Time (days)	Reference	Setup			
									Test type [3]	R_{total} (-)	R_{shaft} (-)	R_{toe} (-)
Borkum Riffgrund 1	A3.2	2.13	45	47.4	38.5	18.0	6.0	Jardine et al (2015)	All	1.5	1.5	1.8
LAXT	1-D44	1.37	25.4	53.9	20.7	15.1	6.0	Bhushan (2004)	Dynamic	1.4	1.5	1.0
″	2-C44	1.37	25.4	53.9	17.7	12.9	1.0	″		1.1	1.1	1.0
″	2-C44	1.37	25.4	53.9	21.4	15.6	75	″		1.6	1.6	1.5
″	3-B44	1.37	25.4	53.9	21.4	15.6	75	″		2.0	2.1	1.6
″	4-D4	1.37	25.4	53.9	21.0	15.4	2.0	″		1.1	1.3	0.7[5]
″	5-C4	1.37	25.4	53.9	20.4	14.9	2.0	″		1.2	1.3	1.1
″	6-B4	1.37	25.4	53.9	20.4	14.9	1.0	″		1.1	1.3	1.0
Nordsee Ost	Metmast	3.35	–	–	–	–	0.04	Kirsch and von Bargen (2012)		1.2		
″	Metmast	3.35	–	–	–	–	0.3	″		1.3		
″	Metmast	3.35	–	–	–	–	31	″		1.5		
Südkai	4A	0.76	12.7	60.0	33.7	44.2	30	Skov and Denver (1988)		1.4		
TTB - P8 bridge pier	P8	1.60	31.3 [4]	51.2	27.0	16.9	3.2	Sawai et al (1996)		1.4	1.5	1.2
TTB - Ventilation tower	R3	2.00	40	50	26.6	13.3	1.8	Shioi et al (1992)		1.3	1.4	1.1
Dunkirk	R1	0.46	13.5	33.9	19.3	42.3	9.0	Jardine et al (2006)	Static T/EoID		1.6	
″	R2	0.46	13.5	33.9	18.9	41.2	235	″	″		3.6	
″	R6	0.46	13.5	33.9	18.9	41.4	81	″	″		2.6	
Larvik	L7-1	0.51	6.3	80.6	20.1	39.6	30	Karlsrud et al (2014)	″ ″		1.9	
″	L2-1	0.51	6.3	80.6	20.1	39.6	131	″	″		2.5	
″	L3-1	0.51	6.3	80.6	20.1	39.6	213	″	″		3.0	
″	L4-1	0.51	6.3	80.6	20.1	39.6	365	″	″		2.8	
″	L5-1	0.51	6.3	80.6	20.1	39.6	729	″	″		2.9	
TTB - P8 bridge pier	P8	1.60	31.3 [4]	51.2	27.0	16.9	75	Sawai (1998)	Static C/EoID	2.4	2.1	?
TTB - Ventilation tower	T	2.00	43 [4]	46.5	30.6	15.3	52	Shioi et al (1992)	″	2.5	3.1	1.4

Notes: (1) t is the wall thickness of the pile tip, (2) L is the embedded length, (3) Static-T: Static Tension, Static-C: Static Compression, (4) includes 9 mm external driving shoe (5) As reported by Bushan (2004). This implausible result is due to assigning a lower proportion of total resistance to the toe during signal matching at BoR compared to EoR which reveals the limitations of signal matching to distinguish shaft resistance near the toe of the pile and true end bearing resistance on the annulus.

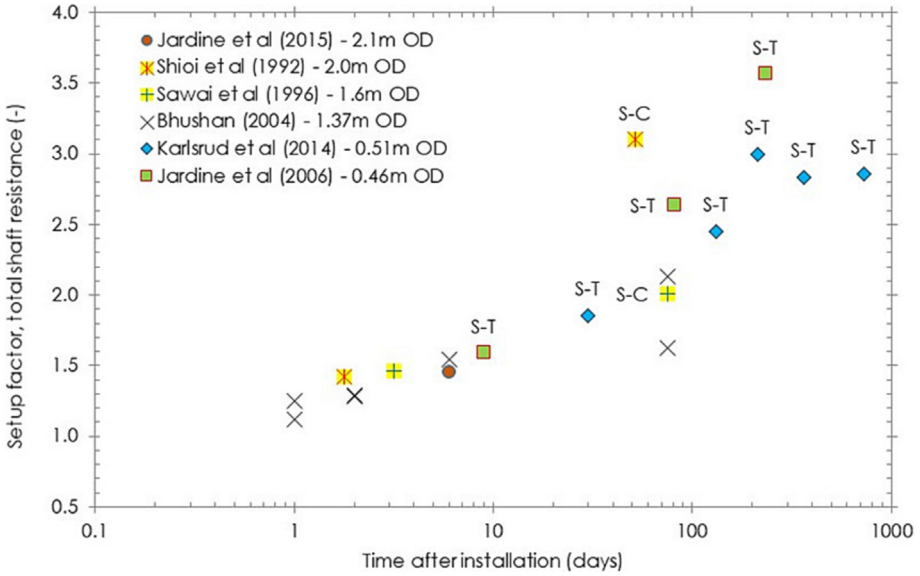

Fig. 3. Shaft resistance setup vs time for open steel piles diameters greater than 0.45 m Note: Impedance of 23,037 kNs/m used for measured velocity presentation.

Table 2
Pile load test database – contents and characteristics.

Project	Pile Ref.	D (m)	t_w (1) (mm)	D/ t_w (-)	L(2) (m)	L/D (-)	$q_{t,avg.}$ (MPa)	$D_{r,\ avg.}$ (%)	Setup time (days)
A	R	2.44	60	40.6	65.8	27.0	48.4	86	3.9
A	T	2.44	60	40.6	65.8	27.0	45.3	83	3.7
B	U	2.48	55	44.3	19.6	7.9	20.9	76	1.0
B	V	2.48	55	45.1	18.6	7.5	28.6	87	8.0
B	W	2.48	70	34.8	25.0	10.1	61.9	100	224
B	X	2.48	50	48.8	28.0	11.3	34.3	87	374
B	Y	2.48	50	49.6	27.0	10.9	35.0	88	340
C	BX	2.13	45	47.4	38.5	18.0	32.8	81	5.8
D	BA	2.59	80	32.4	56.8	21.9	55.9	93	3.2
D	BC	2.59	80	32.4	56.8	21.9	52.5	91	3.1
E	CF	2.44	45	54.2	39.0	16.0	32.8	80	0.3
E	CG	2.44	45	54.2	39.2	16.1	32.8	80	6.2
F(3)	CH	1.37	75	18.3	72.3	52.7	46.3	83	30
G	CL	2.44	55	44.3	47.6	19.5	35.9	80	2.3
G	CM	2.44	55	44.3	47.6	19.5	35.8	80	1.5
H	CN	1.83	50	36.6	28.8	15.7	35.0	87	2.0
I	CO	3.35	50	67.0	35.6	10.6	27.2	76	51
I	CP	3.35	50	67.0	35.6	10.6	27.2	76	51
I	CQ	3.35	50	67.0	35.6	10.6	27.2	76	52
I	CR	3.35	50	67.0	32.6	9.7	44.9	94	82
I	CS	3.35	50	67.0	32.6	9.7	44.9	94	82
I	CT	3.35	50	67.0	32.6	9.7	44.9	94	83
I	CU	3.35	50	67.0	34.6	10.3	44.0	92	52
I	CV	3.35	50	67.0	34.6	10.3	44.0	92	51
J	DN	2.44	60	40.6	45.9	18.8	47.3	90	0.5

Notes: (1) t_w is the wall thickness of the pile tip, (2) L is the embedded length, (3) Project F: thick layers of clay and gravel but significant portion of shaft resistance from sand layer in the deeper section.

brated' or 'refined' wave equation approach is discussed in more detail subsequently.

The PAGE signal matched dynamic base resistances all fell well below those predicted by the ICP-05 or Unified static design methods. Byrne et al. (2012) and Cathie et al. (2020) argue that this discrepancy is due to the relatively low levels of displacement developed under single hammer blows and the different resistance and drainage mechanisms operating under dynamic and static conditions. Although interesting for Soil Resistance to Driving (SRD) predictions, the dynamic toe resistances are not considered further in this paper.

4. Signal matching

4.1. CAPWAP analyses

The CAPWAP (PDI, 2006) signal matching analyses followed Pile Dynamics' (PDI, 2006, 2014) recommended procedures. The assumed end bearing, and shaft resistance distributions, all started from physically credible initial profiles based on Alm and Hamre's (2001) CPT-based approach. CAPWAP radiation damping was adopted to improve the signal matches; Cathie et al. (2022). Consistency was maintained whenever reasonably possible between the shapes of the EoID and BoR shaft resistance distributions, with setup being accommodated by progressive re-scaling and other adjustments to match the recorded signals. All fitting parameters were kept within the recommended (PDI, 2006, 2014) ranges. Fig. 4 provides an example of a measured force and velocity signal, and the fitted upward wave force signal; Wen et al. (2023) provides others.

CAPWAP does not model the internal soil plug but does allow soil below the pile toe to be treated as an additional mass; this feature was activated when found necessary to improve signal matches. As CAPWAP cannot separate internal and external shaft resistance, PAGE considered the overall (total) shaft resistances plus the (effectively annular) end-bearing components. The CAPWAP matches led, as summarised in Table A1 to match quality (MQ – Rausche et al., 2010; PDI, 2006) ranges of 1.4–3.5 and means of 2.3 which signify moderate-to-high matching quality.

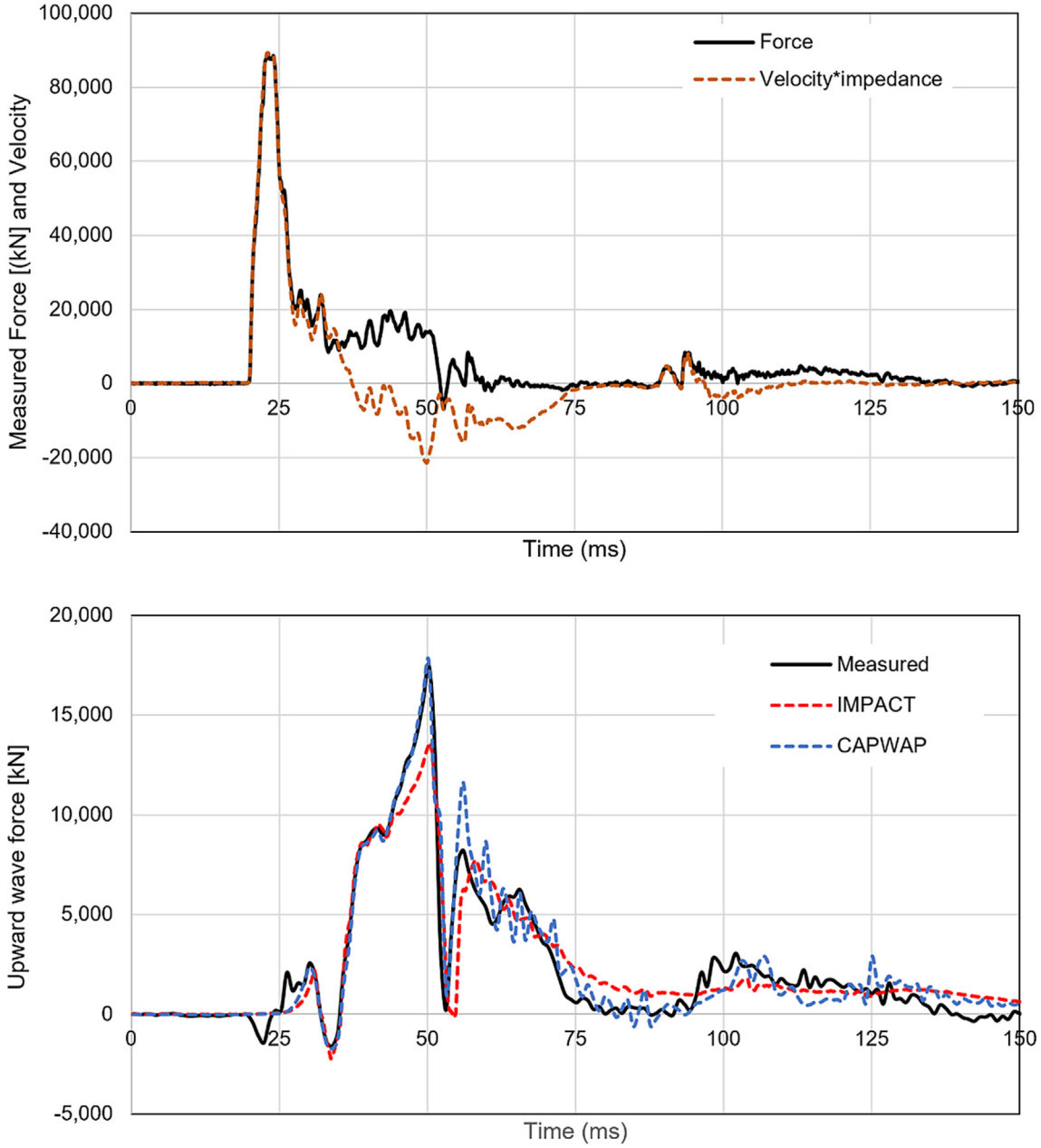

Fig. 4. Examples of signals and signal matching results.

4.2. IMPACT analyses

Parallel signal matching with IMPACT (Randolph, 2008) employed the Randolph and Simons (1986) shaft resistance and Deeks and Randolph (1995) end bearing models, as described by Wen et al (2023). Elastic shear modulus profiles (G_{max}) were derived from correlations with CPT q_t and adjusted by suitable G/G_{max} factors to give operational values for each layer. The initial distributions of shaft resistance and end bearing from which the iterative matching process started were set as in the CAPWAP analyses. Fig. 5a and b show correlations between the interpreted equivalent static axial resistances from IMPACT (R_{IM}) and CAPWAP (R_{CW}) for total resistance (shaft plus base) and overall shaft resistance (external and internal) respectively. The IMPACT values tended to exceed those from CAPWAP, giving R_{IM}/R_{CW} ratios of 1.28 and 1.30 for total and overall shaft resistances respectively and coefficients of variation (CoV) of 0.12 and 0.14. The systematic biases reflect the codes' different rheological

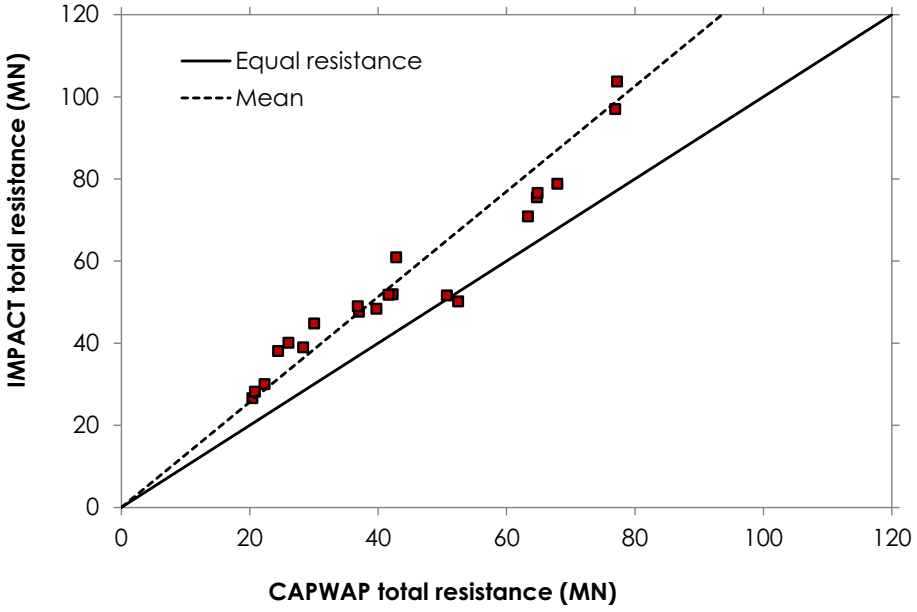

(a) Total resistance

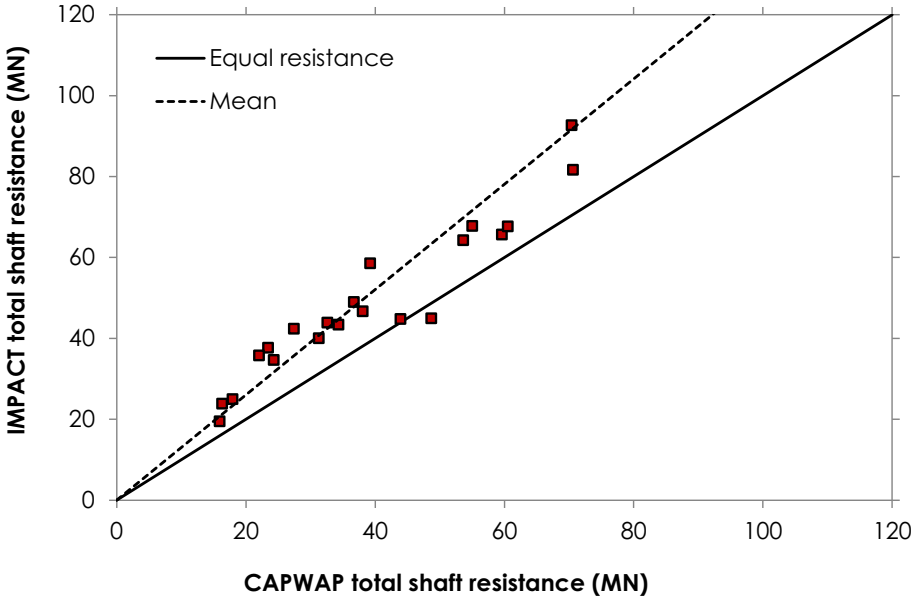

(b) Shaft resistance

Fig. 5. Comparison of CAPWAP and IMPACT axial resistance from signal matching.

models; Wen et al. (2023), Cathie et al. (2022). Unlike CAPWAP, IMPACT models the internal soil plug and external shaft resistance independently through a continuum approach, which Buckley et al. (2020) showed can improve back analyses. The IMPACT analyses indicated that internal shaft resistance contributes 1%–22% (with an 11.3% mean) to the overall PAGE shaft resistances.

4.3. Calibrated wave equation approach

Signal matching can only give representative capacities if the local shaft and tip capacities are mobilised fully under the blows considered (PDI, 2006). CAPWAP analyses of blows involving sets less than approximately 2.5 mm under-estimate ultimate resistance because the CAPWAP result depends on the magnitude of the reflected wave to determine shaft and toe resistance. This restriction does not apply to GRLWEAP analyses which are based on assumed shaft resistance and end bearing profiles, and calculate the resulting set for the given (calibrated) damping and quake parameters (Rausche et al., 2009).

As noted earlier, GRLWEAP wave equation analyses were applied in combination with detailed hammer data to consider the longer term (>50 days) BoR tests with sets < 2.5 mm. The shaft and end bearing resistances derived from signal matching (large set) EoID blows were used to calibrate damping and quake parameters which were then used, with the given hammer characteristics, to develop a bearing graph (SRD v blowcount (set) relationship) and estimate the BoR resistances from low set restrike tests. IMPACT analyses of two cases indicated similar capacities to the calibrated GRLWEAP bearing graph approach (see Appendix Table A1). It appears that IMPACT's continuum approach allows energy dissipation into the soil mass to be captured better than with CAPWAP; the good agreement justified including the GRLWEAP results in the PAGE dataset. These data are considered of lower reliability than direct signal matching on blows for which the full shaft and end bearing resistance was mobilised, but still provide a credible indicator of the resistance at the time of restrike, particularly in view of the concordance with the IMPACT signal matching results in which the dynamic response of the soil mass is captured even at low sets.

4.4. Ageing trends for shaft and total resistance

The dynamic PAGE offshore dataset trends for overall shaft resistance and total resistance setup, S,are plotted in Fig. 6a and 6b against $\log_{10}$ time after driving. The setups (listed in Table A1) are defined as the ratio of the BoR (R_{BoR}) to EoID (R_{EoID}) resistances.

Only marginal resistance growth (≈10%) is evident over the first 12 h. The rate of change builds to a maximum after ≈3 days and then declines to around zero within a month and appears to reach a mean shaft setup plateau of 1.96 after 20–30 days. It is recognised that the dataset includes relatively few restrikes at ages > 50 days. The longer term restrikes came from just two Projects (B and I – see Table A1) and the GRLWEAP (confirmed by IMPACT) approach was required for one of these cases. It is also recognised that other trends might emerge from static offshore tests or BoR tests conducted at a broader range of sites and, where necessary, with larger hammers. However, Fig. 6 represents the only high-quality, public domain, long-term dynamic or static tests on large offshore piles driven in sands of which the authors are aware.

A generic hyperbolic expression (Equation (1) fits these data with the parameters summarised in Table 3. Note that t = time since EoID in days; the reference value of 3 days is a fitting parameter that corresponds to the time at which the rate of gain is greatest.

$$y = A + B \times \tanh(C \times (t - 3)) \quad (1)$$

Where:

y = setup factor (S) or normalised resistance ($R_{shaft,m}/R_{shaft,c}$).

A = y-value 3 days after installation

B = maximum increase of y-value beyond 3 days (A + B defines the plateau).

C = parameter controlling the slope of tanh function at 3 days.

4.5. Normalised ageing trends

Calculations were undertaken to allow the PAGE EoID and BoR signal matching results to be compared with static axial shaft resistances from the "full" ICP-05 (R_{ICP-05}) and Unified ($R_{UNIFIED}$) methods. Figs. 7a and 7b present ageing trends for the PAGE offshore piles' overall EoID and BOR shaft resistances normalised by the two methods, with the EoID points plotted at nominal 0.1 day ages to aid visualisation. The PAGE data show an average EoID ratio of 0.52 compared to ICP-05 predictions and tend, serendipitously, towards a steady and close match with the ICP-05 capacities 20–30 days after driving. The best-fit curve, described by Equation (1) and Table 3, gives a CoV of 0.23, similar to that found for ICP-05 predictions when evaluated against static test databases involving generally smaller piles (Jardine et al., 2005; Yang et al., 2017; Lehane et al., 2017).

The corresponding Unified method plot and best fit trend curve shown in Fig. 7b) indicates an average EoID ratio of 0.70, and an average BoR ratio of 1.35 at ages exceeding 30 days. The PAGE overall shaft resistance curve matches the Unified predictions at an age ≈4 days and shows a CoV of 0.22.

4.6. Comparison with earlier studies

4.6.1. Additional analyses

Dynamic analyses were made for PAGE of the cases summarised in Table 4 which involved static and dynamic

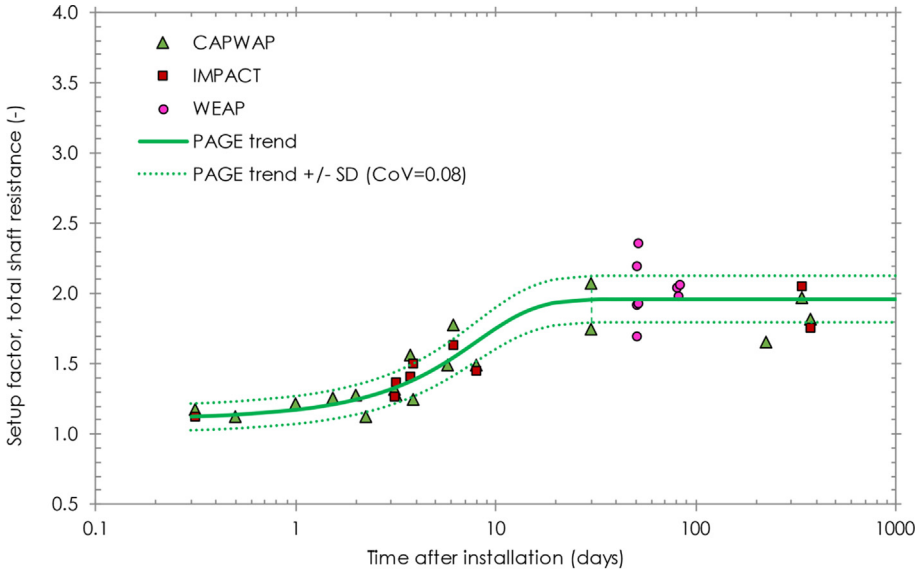

a) Total shaft resistance setup

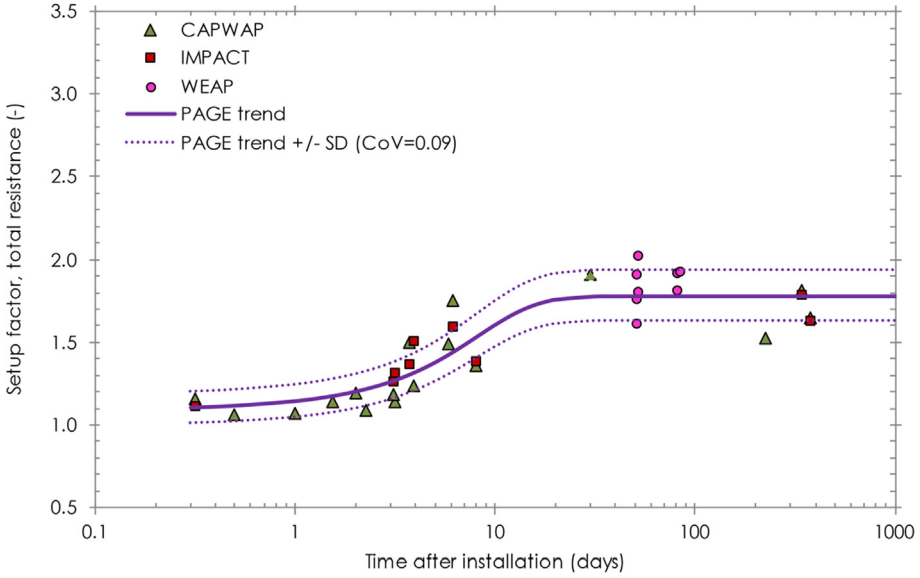

b) Total resistance setup

Fig. 6. Development of setup with time, offshore PAGE dataset only.

Table 3
PAGE setup trend fitting parameters.

Parameter evaluated	A	B	C	Reference
Total shaft resistance setup factor	1.32	0.640	0.1174	Fig. 6a
Total resistance setup factor	1.26	0.520	0.1155	Fig. 6b
ICP normalised total shaft resistance	0.677	0.323	0.1705	Fig. 7a
Unified normalised total shaft resistance	0.904	0.446	0.1504	Fig. 7b

testing at various ages on 0.76–2.0 m diameter open steel piles. The results are provided in Table A2.

Wen et al. (2023) report the first dynamic analyses of the 762 mm OD EURIPIDES piles, which were driven in 1995 near Eemshaven in The Netherlands. Three of the four static tests were conducted after some days of uninterrupted ageing, following many metres of continuous driving. The 533-day experiment followed a test conducted after 6-days and so may have under-estimated the resistance available to an undisturbed 'virgin' pile at the same

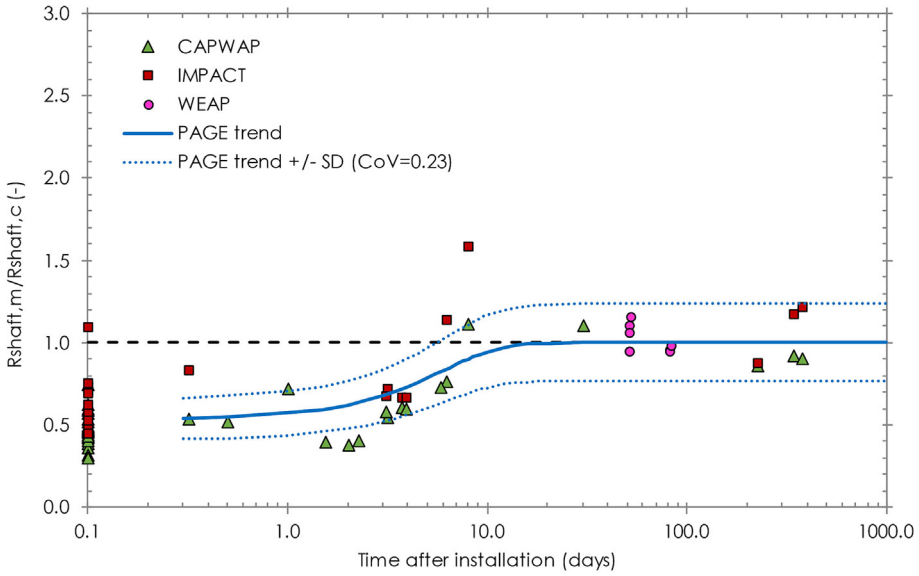

Fig. 7a. Development of normalised total shaft resistance with time, offshore PAGE dataset only, normalised by ICP-05 predictions.

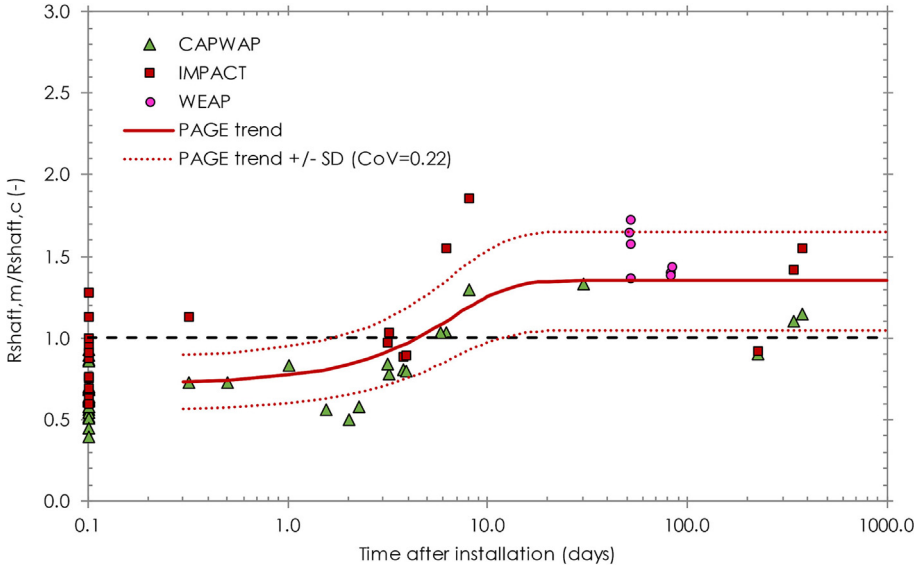

Fig. 7b. Development of normalised total shaft resistance with time, offshore PAGE dataset only, normalised by Unified method predictions Notes: 1) S-T and S-C refer to setup based on EoD interpreted shaft resistance combined with tension or compression shaft resistance, respectively, from static tests after setup; 2) CW – CAPWAP, IM-IMPACT signal matching.

Table 4
Case studies - main characteristics.

Project	Pile Ref.	D (m)	t_w (1) (mm)	D/t_w (-)	L(2) (m)	L/D (-)	Setup time (days)
EURIPIDES	Loc1_CP1	0.76	35.55	21.5	30.5	40.0	7
EURIPIDES	Loc1_CP2	0.76	35.55	21.5	47.0	61.6	12
EURIPIDES	Loc2_CP1	0.76	35.55	21.5	46.7	61.2	6
EURIPIDES	Loc2_CP2	0.76	35.55	21.5	46.2	61.5	533
Horstwalde	1B	0.71	25.00	28.4	17.6	24.8	546
Horstwalde	4D	0.71	25.00	28.4	17.7	24.8	30
TTB	T	2.00	43.00 (3)	46.5	30.6	15.3	52
TTB	P8	1.60	31.25 (3)	51.2	27.0	16.9	75

Notes: (1) t_w is the wall thickness of the pile tip, (2) L is the embedded length, (3) including 9 mm external driving shoe.

age. However, Galvis-Castro et al. (2019) found that the impact on shaft capacity in sand of prior static compression tests (and by inference low set re-strikes) is less severe than that found after tension testing by Jardine et al. (2006) and Karlsrud et al. (2014). Also, the 527-day pause between the EURIPIDES pile's tests may have allowed the impact on its relatively 'young' 6-day capacity to have been largely overwritten by in-situ ageing processes.

BAM (2014) report dynamic and static axial compression and tension tests, as well as axial cyclic loading tests on 711 mm OD open-tubular steel piles impact driven in predominantly medium dense to very dense sands at Horstwalde, Germany. Driving data from two piles were re-analysed for PAGE along with 30 and 546-day re-strikes. However, the 30-day case followed a prior 10-day re-strike, while the 546-day test followed 13 and 39-day restrikes. The Horstwalde and 533-day EURIPIDES re-strikes provide lower bounds to the capacities that 'virgin' piles might show at the same ages.

Static and dynamic load testing was also conducted between 1989 and 1992 for the Trans-Tokyo Bay Highway (TTB) project on open steel piles driven predominantly in sands and silts, although clay layers were also present (Shioi et al., 1992; Sawai et al., 1996). The tests contributed the only D > 0.81 m case in the Chow (1997), Jardine et al. (2005), Lehane et al. (2017) and Yang et al. (2017) test databases. Independent signal matching by PAGE of the 2.0 m OD Pile T's EoID resistance allowed its setup to be evaluated from a 52-day age, static compression test. Independent signal matching was also performed on P8, a 1.6 m OD pile, which had an extensive array of strain gauges and accelerometers along its embedded length. Data from Sawai (1998) were re-analysed to establish the dynamic resistance under EoID conditions, which was compared with a static test conducted 75 days after driving. It is important to note that enlarged external driving shoes were fitted to both piles that were proven, in parallel tests, to have reduced their driving resistances.

4.6.2. Synthesis

Results from the three additional case histories summarised in Tables 4 and Table A2, are plotted on Fig. 8 together with the PAGE offshore pile setup trend curve (from Fig. 6) and the earlier discussed data from Shioi et al. (1992), Sawai et al. (1996), Bhushan (2004), Jardine et al. (2006) (2015) and Karlsrud et al. (2014).

The onshore/nearshore dynamic and static test data agree with the PAGE offshore pile trends up to 20–30 days. However, they show setup continuing to build to normalised levels far greater than those established for the PAGE offshore piles. While the dynamic tests on larger onshore and nearshore piles fall closest to the PAGE piles' plateau, the tests on ≈500 mm OD piles at Dunkirk (Jardine et al., 2006) and Larvik (Karlsrud et al., 2014) deviate furthest from it. The 545-day age test on a 710 mm OD Horstwalde pile indicated dynamic shaft setup factors of 2.36 to 2.40 (from IMPACT and CAPWAP respectively) that plot well above the offshore plateau, despite the pile's earlier re-strikes.

As noted earlier, the enlarged external driving shoes employed for the Trans Tokyo Bay (TTB) piles reduced their EoID shaft resistances and the mean of the 0.56 and 0.34 shaft $R_{EoID}/R_{ICP\text{-}05}$ ratios found for the 1.6 m and 2.0 m piles, respectively, falls 13% below the mean from the PAGE offshore dataset. However, the external shoes appear to have had less impact on the piles' long-term capacities, giving $R_{Static\text{-}comp}/R_{ICP\text{-}05}$ ratios of 1.3 and 1.01 in the 56-day and 52-day tests on the 1.6 m and 2.0 m piles respectively. These outcomes boosted the TTB piles' setup ratios; similarly sized piles driven without enlarged external shoes could be expected to show lower setup.

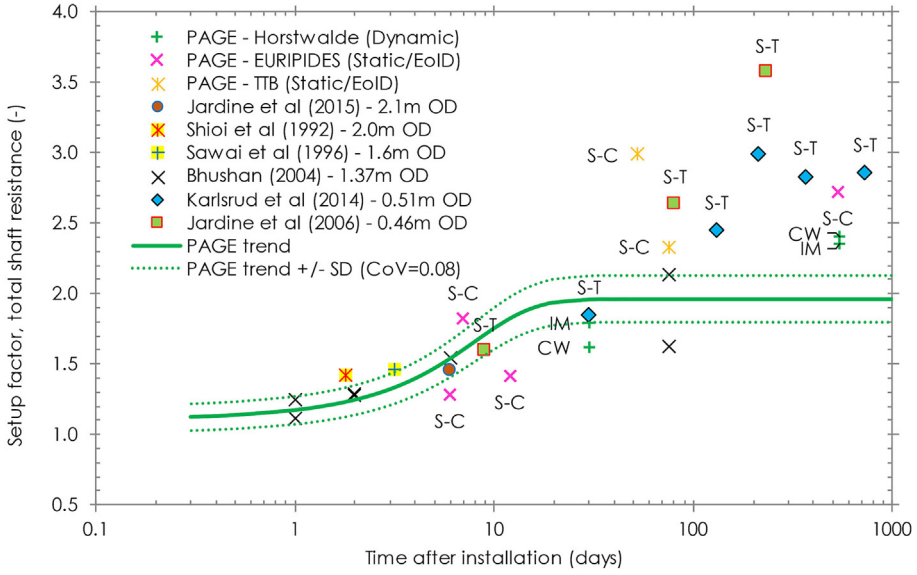

Fig. 8. Development of total shaft resistance setup with time, offshore PAGE dataset only.

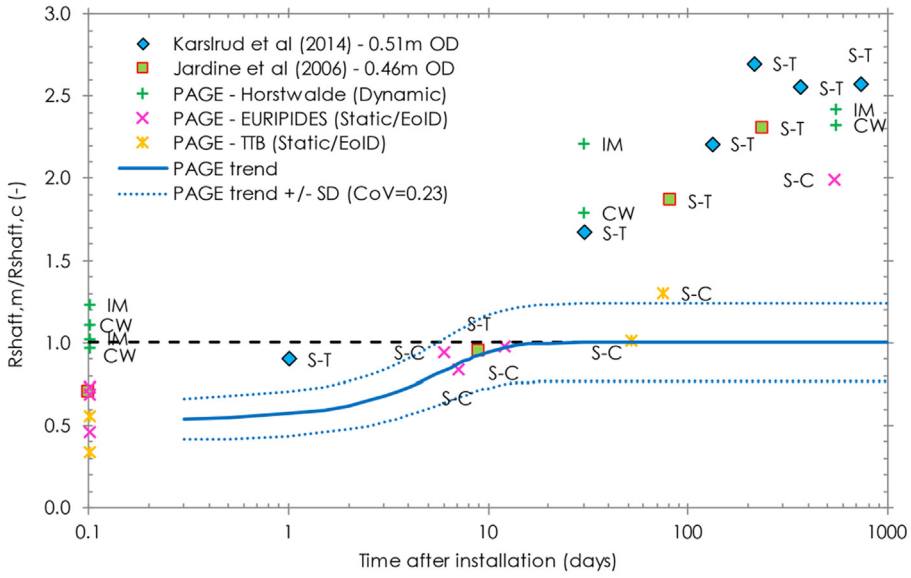

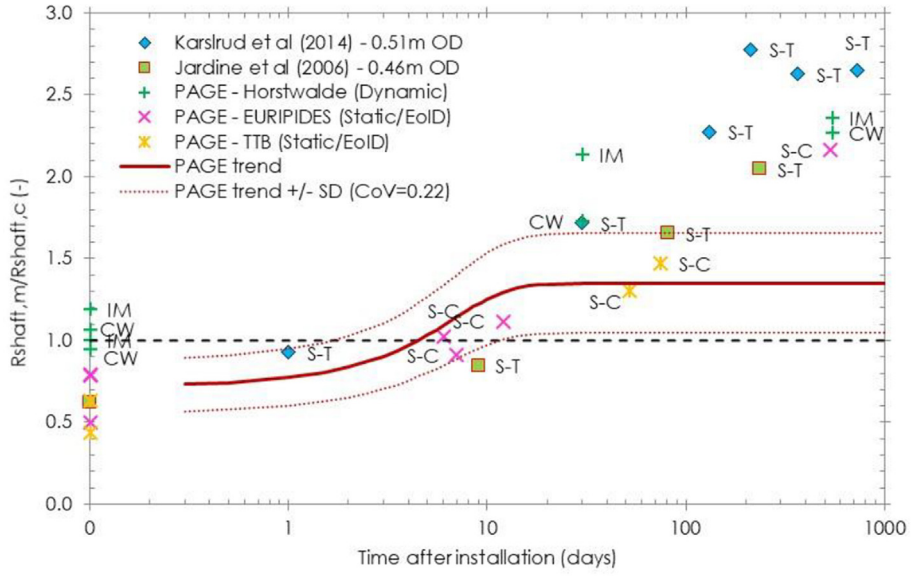

Fig. 9. Development of normalised total shaft resistance with time, offshore PAGE dataset with 'other data' cases.

Fig. 9a and 9b compare the additional case histories' ICP-05 and Unified method normalised shaft resistance plots, along with the PAGE offshore pile trends from Fig. 7. The 2 m and 1.6 m OD (nearshore) TTB piles' long-term tests fall closer to the PAGE offshore trend than all the other ($D \leq 762$ mm) data points, which plot well above the mean PAGE offshore trend.

5. Discussion

The combined datasets shown in Figs. 6 to 9 show that all piles, with diameters from 0.45 m to 3.5 m, experienced a doubling of dynamic and/or static shaft capacities over their first 20 days after driving. The mechanisms hypothesised by Jardine et al. (2006) to cause such trends included two that are independent of pile material:

- Interface shearing resistances increasing by 10 to 15% through any cold-welding bonding of sand grains to the shaft, leading to δ approaching $\varphi'_{critical\ state}$.
- Increases in the shaft radial effective stresses through creep weakening the circumferential arching that modelling and calibration chamber tests identify as applying

after driving (Jardine, 2020). Any such creep processes would naturally slow as any cementing developed around the pile shafts.

These hypotheses remain to be verified for offshore-scale steel piles though reliable local radial effective stress measurements. While, as noted in the introduction, the 'creep-arching' mechanism was proven to be ineffective around 36 mm OD laboratory model and 50 mm OD field micro-piles, Jardine (2020) argued that the crushed sand shear zone reported by Yang et al. (2010) may lead to the creep-arching mechanism only being effective with larger diameter piles and potentially depending on D/t_w. If so, this mechanism may explain why the dynamic and static normalised capacity trends shown by 0.45 to 3.5 m OD piles tend to converge after 20 days. This feature also indicates that the markedly divergent ageing behaviours shown by smaller onshore and larger offshore piles at greater ages are unlikely to be due to any fundamental difference between dynamic and static shaft capacity measurements, or offshore driving practice. The later age divergence also appears too systematic to be explained as resulting from uncertainty in the carefully double-checked and quality-assured PAGE signal matching analyses.

The remaining postulated ageing mechanisms involve pile geometry, including diameter, and steel corrosion processes. Considering geometry first, recent offshore practice has tended towards driving larger diameter, relatively stubby, piles. This is reflected in the PAGE piles' having $7.5 \leq L/D \leq 27.0$ ratios, with just one ($L/D = 52.7$) exception. The smaller diameter onshore test piles (at Dunkirk, Larvik, Euripides and Horstwalde, see Tables 1 and 4) covered a $24.8 \leq L/D \leq 61.6$ range that is more typical of historical offshore practice. While checks made within the two datasets did not identify L/D as an influential factor, Fig. 10 shows that the ratio of measured shaft capacity to that predicted (in this case by ICP-05) correlates negatively with pile diameter D, as well as increasing strongly with age after driving for cases with $D < 1.5$ m, as was emphasised earlier in Figs. 2, 3, 8 and 9. This dependence on diameter is discussed further below.

Carroll et al. (2020) show how mild steel micro-piles driven at onshore sites corrode over the months after driving and develop rough crusts with sand grains cemented to their shafts. Kolk et al. (2005) reported the same features around the 762 mm diameter EURIPIDES pile and Ohsaki (1982) quantified rates of steel loss, reporting broadly similar rates of thickness loss per year under a wide range of ground conditions. Corrosion reaction rates are independent of pile diameter but could be different at offshore sites due to their generally less favourable (lower) groundwater temperatures and dissolved oxygen levels, although the water's salinity would accelerate corrosion.

Applying the ICP-05 approach shows how corrosion can be expected to make a diameter-dependent contribution to setup. The local radial effective stresses acting on the pile shaft at failure in compression and tension are defined by Equations (2) and (3), respectively:

$$\sigma'_{rf,c} = \sigma'_{rc} + \Delta\sigma'_{rd} \tag{2}$$

$$\sigma'_{rf,t} = 0.9(0.8\sigma'_{rc} + \Delta\sigma'_{rd}) \tag{3}$$

where: σ'_{rf} is the local radial effective stress, given as a function of CPT resistance, overburden pressure and pile geometry and $\Delta\sigma'_{rd}$ is the dilatant increase in local radial effective stress during pile loading, which is related to sand shear stiffness and outward radial interface displacements:

$$\Delta\sigma'_{rd} = 4G\frac{\Delta r}{D} \tag{4}$$

where: G is the sand's small-strain shear modulus, evaluated according to Baldi et al. (1989), D the pile diameter

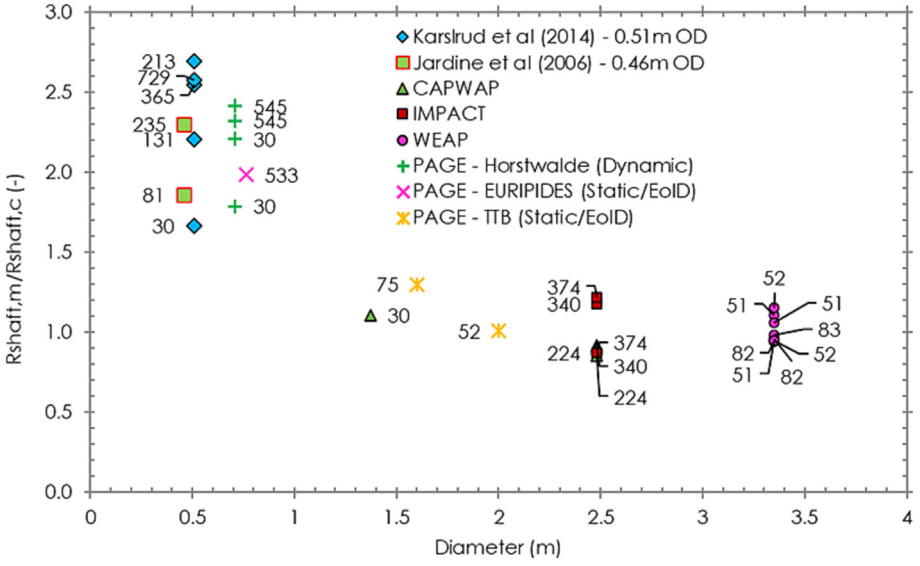

Fig. 10. Dependence on pile diameter of total shaft capacities of all piles tested at ages greater than 30 days, offshore PAGE dataset combined with 'other data' cases.

and Δr is the radial interface displacement, taken as twice R_{CLA}, the pile shaft Centre-Line-Average roughness. Δr is generally assumed to be 0.02 mm for lightly rusted steel piles at the time of driving. Pile roughness increases associated with even minor pitting can be expected to cause greater dilation within the interface shear zone under axial loading. Rearrangement of the sand fabric close to the pile shaft through creep and corrosion product migration into the shear zone could also enhance the dilation developed at the interface. The products may initially displace water, occupy pore spaces and cement the sand to the shaft. However, once the pores become blocked continuing corrosion may start to displace the sand mass radially outwards. Equation (4) shows that the impact on σ'_{rf} of any additional radial displacement Δr caused by dilation, or radially outward growth of pile corrosion product, is directly proportional to the operational G and inversely proportional to D. Although G may fall as the displacements and 'cavity strains' $\varepsilon_c = 2\Delta r/D$ grow, the resulting changes in σ'_{rf} will still fall steeply with D.

Parametric analyses applying the 'full' ICP-05 methodology to the offshore dataset can test the enhanced radial effective stress hypothesis. The mean relative density (86%), pile length (40 m) and D/t_w (50) applying to the PAGE piles offers a suitable baseline set to explore the variable impact on total shaft resistance R_{shaft} of different values of Δr applying to piles with a wide range of outside pile diameters, D. Fig. 11 plots against pile diameter the shaft resistance predictions made for Δr values up to 0.4 mm, normalised by the default (Δr = 0.02 mm) case and Fig. 12 illustrates the results in an indicative way by overlaying the curves over the appropriate PAGE dataset. This broad comparison does not address the possible effects on set-up of variations between the sand profiles, L/D or D/t_w ratios. However, the curves found with Δr values of 0.04 to 0.4 mm match the pile test dataset's strong correlations with diameter and age after driving.

Lings and Dietz (2005) report from laboratory interface shear tests that the normal displacements (equivalent to Δr) associated with the shaft interface shear failure mechanism switch from a 'partially rough' to a 'fully rough' mode, which applies once the interfaces' R_{CLA} values rise (through corrosion and sand bonding) to exceed $d_{50}/10$. The dilatant normal displacements were shown to grow from values around $2R_{CLA}$ for partially rough interfaces to give total dilations of 1.35 to 2.15 d_{50} (falling with grain size) by the stages at which shearing against fully rough ($R_{CLA} > d_{50}/10$) interfaces had led to fully critical state conditions. R_{CLA} would only have to increase by 5 μm to 20 μm to induce 'rough' shearing with Δr values of 0.2 to 0.6 mm in typical North Sea sands (which show 0.15 mm to 0.3 mm d_{50} ranges) according to the results from Lings and Dietz's tests. These potential Δr values marginally exceed the 0.1 to 0.4 mm range required to explain the capacity trends as indicated in Fig. 12. Closer estimates could be obtained for any given site through representative shear tests involving fully rough interfaces.

It appears feasible that corrosion and/or cold-weld cementing to the pile shafts could lead to a gradual shift over time from partially to fully rough shaft shearing behaviour that boosts the dilation induced around piles under loading and explains the field shaft capacity-diameter trend

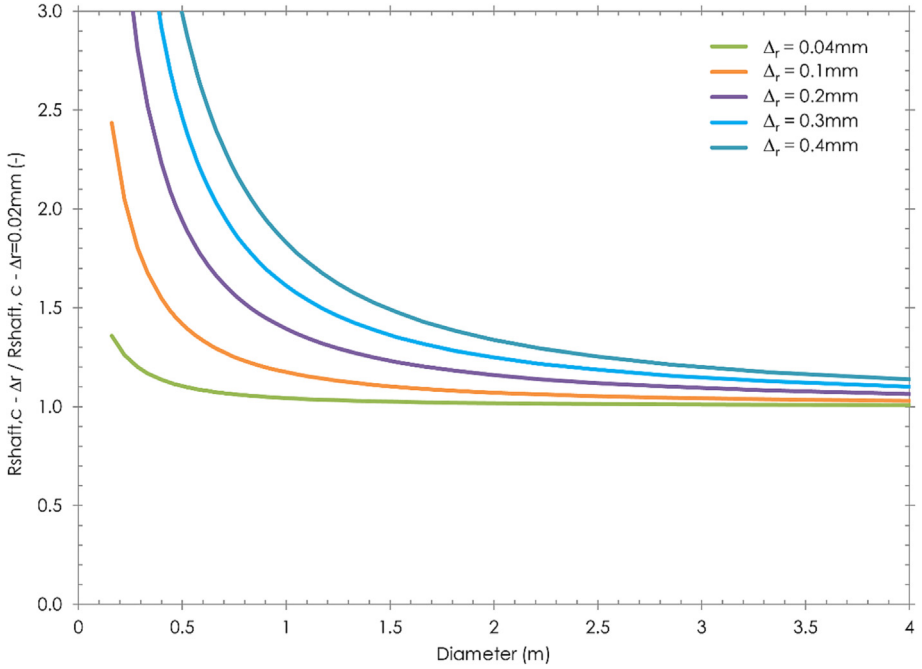

Fig. 11. Contribution of enhanced dilation to shaft resistance as a function of pile diameter for various Δr values considering mean PAGE offshore dataset L = 40 m, D/t_w = 50, D_r = 86% values, normalised by shaft resistance calculated with default ICP-05 Δr = 0.02 mm.

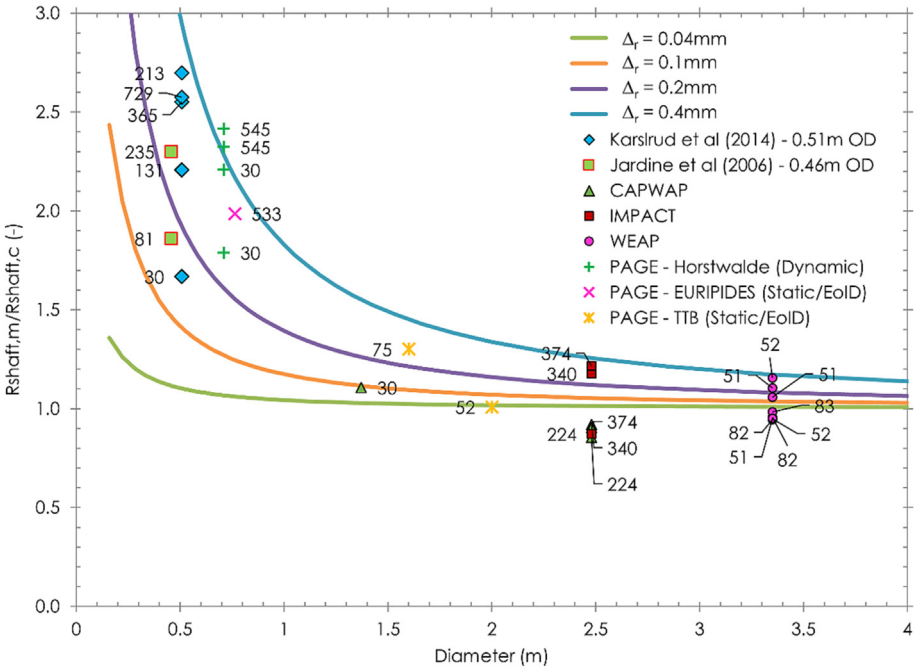

Fig. 12. PAGE offshore dataset overlying parametric analyses (Fig. 11) showing how enhanced dilation may explain diameter dependence of long-term ageing.

shown in Fig. 10 as resulting from Δr gradually increasing up towards fully rough values through corrosion and bonding developing over time around the pile shafts.

As noted in the introduction, Axelsson (2000) and Gavin et al. (2015) reported field observations of dilation related components of shaft resistance increasing markedly with age around steel and concrete piles. Static tests on large (D > 1 m) piles (or in their absence, further dynamic tests on large diameter piles with ages greater than 30 days) are required to confirm the interpreted diameter dependent ageing mechanism. Research into the kinetics of corrosion around pile shafts under various conditions, and their impact over time on shaft radial effective stress conditions would also be valuable. Until then, working hypotheses that are compatible with the pile test datasets considered by PAGE are:

(i) The early ageing behaviours of piles are dominated by increases in the relevant angles of shearing resistance, particle bonding and/or stress re-distribution mechanisms that lead to similar outcomes for piles with 0.45 to 3.5 m ODs, although less setup around smaller diameter micro-piles. These gains appear to be already accounted for in current CPT based design methods,

(ii) Ageing at ages greater than 20 to 30 days is driven by corrosion or cold-welding processes whose consequences reduce systematically with diameter in a manner that is consistent with corrosion and sand grain bonding gradually inducing fully rough conditions at the pile-sand interface and the radial 'dilative' displacements Δr induced by shearing to failure increasing from ≈20 μm to 0.1–0.4 mm.

(iii) The impact of raised Δr values may be gauged by substitution into Equation (4) and application in the ICP-05 or Unified design methods; site specific Δr values may be established through representative laboratory tests.

(iv) Further slow long-term capacity gains could apply to fully rough piles through corrosion products expanding radially outwards after blocking the pore spaces around the pile shafts.

6. Summary and conclusions

The PAGE JIP applied strict quality assurance criteria in building a dataset of 25 large offshore piles for which end-of-initial driving (EoID) and beginning-of-restrike (BoR) blows could be analysed to obtain resistances after known setup periods. These cases were complemented by re-analyses of nearshore/onshore tests where dynamic impact and static testing had been conducted on open steel piles. The long-term offshore and nearshore ageing trends allow four main conclusions:

1. Static and dynamic tests on piles with diameters from 0.45 m to 2 m show comparable aged capacity trends, with setup factors that tend to reduce with pile diameter.
2. Dynamic tests on large offshore piles, with diameters up to 3.4 m, follow similar initial ageing trends, with shaft capacities approximately doubling over the first 20 to 30 days after driving.
3. The longer-term trends shown by large offshpre piles diverge markedly from those shown by smaller onshore piles at ages greater than 30 days. Piles with diameters greater than 1 m driven offshore appear to show little or no additional set up, while smaller diameter onshore piles tested statically or dynamically show shaft capacities growing markedly over the next year.

4. Potential mechanisms have been proposed for the piles' early ageing behaviours. Diameter-dependent radial stress increases due to enhanced dilation under axial loading provide a credible explanation for the diverging long-term setup trends of the large offshore and smaller onshore piles. The effects of this process on long term capacity can be addressed by revising the values of Δr substituted into the ICP-05 or Unified axial shaft capacity methods' interface dilation expressions.

The PAGE dynamic test analyses provide the only public domain summary of how the field capacities of large open steel tubular offshore piles driven in sand vary with time. The outcomes have important implications for offshore pile foundation axial capacity prediction and assessment. Large-scale static tests conducted over greater ageing durations, or additional analyses of dynamic re-strikes made on aged piles with sufficiently large hammers, provide the only means of complementing the PAGE analyses and establishing more reliable field ageing trends.

Acknowledgements

PAGE was executed by Cathie Group and Geotechnical Consulting Group, sponsored by BP, DEME Offshore, EnBW, Equinor, Jan de Nul, Scottish Power Renewables, Van Oord and Ørsted, and supported by a review panel consisting of Jens Bergan-Haavik (DNV GL), Dr Oswald Klingmuller (GSP), Dr Neil Morgan (Lloyds Register), Dr Frank Rausche (Pile Dynamics Inc) and Prof. David White (University of Southampton). Their support is gratefully acknowledged. We also acknowledge gratefully other team members: Chiara Prearo, Erdem Ozsu (Cathie), Kai Wen (Imperial College) and Dr Tingfa Liu (University of Bristol).

Appendix A

See Tables A1 and A2.

Table A1
Signal matching results.

Project	Pile Ref.	D (m)	L (m)	EoID/BoR	Enthru (MJ)	Set (mm)	Time (days)	Analysis type[1]	R_{total} (MN)	R_{shaft} (MN)	R_{toe} (MN)	Setup		
												S_{total} (-)	S_{shaft} (-)	S_{toe} (-)
A	R	2.44	65.8	EoID	1374	10.1	–	CW	52.5	48.7	3.7			
A	R	2.44	65.8	EoID	1374	9.3	–	IM	50.2	45.0	5.2			
A	R	2.44	65.8	BoR	1530	3.8	3.9	CW	64.7	60.5	4.2	1.23	1.24	1.14
A	R	2.44	65.8	BoR	1530	3.9	3.9	IM	75.5	67.7	7.8	1.50	1.50	1.50
A	T	2.44	65.8	EoID	1422	10.1	–	CW	42.3	38.1	4.2			
A	T	2.44	65.8	EoID	1421	8.9	–	IM	51.9	46.7	5.2			
A	T	2.44	65.8	BoR	1305	6.7	3.7	CW	63.3	59.6	3.7	1.50	1.57	0.88
A	T	2.44	65.8	BoR	1305	6	3.7	IM	70.9	65.7	5.2	1.37	1.41	1.00
B	U	2.48	19.6	EoID	395	8.3	–	CW	14.8	8.7	6.1			
B	U	2.48	19.6	BoR	568	7.5	1.0	CW	15.8	10.6	5.2	1.07	1.22	0.85
B	V	2.48	18.6	EoID	755	11	–	CW	20.8	16.3	4.5			
B	V	2.48	18.6	EoID	755	12	–	IM	28.2	23.9	4.3			
B	V	2.48	18.6	BoR	684	4.5	8.0	CW	28.3	24.3	4.0	1.36	1.49	0.89
B	V	2.48	18.6	BoR	684	4.8	8.0	IM	39.0	34.7	4.3	1.38	1.45	1.00
B	W	2.48	25.0	EoID	799	8.1	–	CW	33.3	26.6	6.7			
B	W	2.48	25.0	BoR	912	5	224	CW	50.7	43.9	6.8	1.52	1.65	1.01
B	W	2.48	25.0	BoR	912	5.3	224	IM	51.7	44.8	6.9			
B	X	2.48	28.0	EoID	657	8.2	–	CW	22.3	17.9	4.4			
B	X	2.48	28.0	EoID	657	7.7	–	IM	30.1	25.0	5.1			
B	X	2.48	28.0	BoR	449	5	374	CW	36.8	32.6	4.2	1.65	1.82	0.95
B	X	2.48	28.0	BoR	449	4.3	374	IM	49.0	43.9	5.1	1.63	1.76	1.00
B	Y	2.48	27.0	EoID	668	10.0	–	CW	20.4	15.9	4.5			
B	Y	2.48	27.0	EoID	668	11.5	–	IM	26.6	19.5	7.1			
B	Y	2.48	27.0	BoR	992	10.0	340	CW	37.0	31.3	5.7	1.81	1.97	1.27
B	Y	2.48	27.0	BoR	992	10.7	340	IM	47.7	40.0	7.6	1.79	2.05	1.07
C	BX	2.13	38.5	EoID	640	10.0	–	CW	25.0	20.7	4.3			
C	BX	2.13	38.5	BoR	713	2.0	5.8	CW	37.2	30.8	6.4	1.49	1.49	1.49
D	BA	2.59	56.8	EoID	1674	11.4	–	CW	67.9	55.0	12.8			
D	BA	2.59	56.8	EoID	1674	12.2	–	IM	78.8	67.8	11.0			
D	BA	2.59	56.8	BoR	1817	5.0	3.2	CW	77.2	70.4	6.8	1.14	1.28	0.53
D	BA	2.59	56.8	BoR	1817	5.3	3.2	IM	103.7	92.7	11.0	1.32	1.37	1.00

(*continued on next page*)

Table A1 (*continued*)

Project	Pile Ref.	D (m)	L (m)	EoID/BoR	Enthru (MJ)	Set (mm)	Time (days)	Analysis type[1]	R_{total} (MN)	R_{shaft} (MN)	R_{toe} (MN)	Setup		
												S_{total} (-)	S_{shaft} (-)	S_{toe} (-)
D	BC	2.59	56.8	EoID	1801	9.1	–	CW	64.8	53.6	11.1			
D	BC	2.59	56.8	EoID	1801	11.4	–	IM	76.6	64.3	12.2			
D	BC	2.59	56.8	BoR	1713	4.4	3.1	CW	76.9	70.6	6.3	1.19	1.32	0.57
D	BC	2.59	56.8	BoR	1713	3.8	3.1	IM	97.0	81.7	15.3	1.27	1.27	1.25
E	CF	2.44	39.0	EoID	591	8.5	–	CW	26.0	23.4	2.6			
E	CF	2.44	39.0	EoID	591	8.8	–	IM	40.1	37.7	2.4			
E	CF	2.44	39.0	BoR	714	10.0	0.3	CW	30.0	27.4	2.6	1.15	1.17	1.00
E	CF	2.44	39.0	BoR	714	9.6	0.3	IM	44.8	42.4	2.4	1.12	1.12	1.00
E	CG	2.44	39.2	EoID	793	11.6	–	CW	24.4	22.0	2.4			
E	CG	2.44	39.2	EoID	793	11.5	–	IM	38.1	35.8	2.4			
E	CG	2.44	39.2	BoR	727	7.0	6.2	CW	42.8	39.2	3.6	1.75	1.78	1.50
E	CG	2.44	39.2	BoR	727	6.8	6.2	IM	60.9	58.6	2.4	1.60	1.64	1.00
F	CH	1.37	72.3	EoID	1046	12.7	–	CW	24.6	21.4	3.3			
F	CH	1.37	72.3	BoR	1321	6.8	30	CW	47.0	44.2	2.8	1.91	2.07 (1.75[1])	0.86
G	CL	2.44	47.6	EoID	516	10.0	–	CW	24.7	21.2	3.5			
G	CL	2.44	47.6	BoR	613	10.0	2.3	CW	26.9	23.9	3.0	1.09	1.13	0.86
G	CM	2.44	47.6	EoID	575	9.2	–	CW	22.5	18.6	3.9			
G	CM	2.44	47.6	BoR	664	10.0	1.5	CW	25.6	23.3	2.3	1.14	1.25	0.59
H	CN	1.83	28.8	EoID	377	9.0	–	CW	10.8	8.2	2.6			
H	CN	1.83	28.8	BoR	377	1.0	2.0	CW	12.9	10.5	2.4	1.19	1.28	0.92
I	CO	3.35	35.6	EoID	1334	10.0	–	CW	39.8	32.9	6.9			
I	CO	3.35	35.6	BoR	1134	1.7	51	WEAP	70.2	63.3	6.9	1.76	1.92	1.00
I	CP	3.35	35.6	EoID	1098	8.7	–	CW	40.5	35.8	4.7			
I	CP	3.35	35.6	BoR	1064	2.3	51	WEAP	65.3	60.6	4.7	1.61	1.69	1.00
I	CQ	3.35	35.6	EoID	1276	7.7	–	CW	39.7	34.3	5.4			
I	CQ	3.35	35.6	EoID	1276	9.2	–	IM	48.4	43.4	5.0			
I	CQ	3.35	35.6	BoR	1202	2	52	IM	75.2	67.7	7.5	1.55	1.56	1.50
I	CQ	3.35	35.6	BoR	1202	2	52	WEAP	71.6	66.2	5.4	1.80	1.93	1.00
I	CR	3.35	32.6	EoID	1297	6.5	–	CW	41.6	36.7	4.9			
I	CR	3.35	32.6	EoID	1297	6.6	–	IM	51.8	49.0	2.8			
I	CR	3.35	32.6	BoR	1091	0.2	82	IM	104.2	101.4	2.8	2.01	2.07	1.00
I	CR	3.35	32.6	BoR	1091	0.2	82	WEAP	79.8	74.9	4.9	1.92	2.04	1.00
I	CS	3.35	32.6	EoID	1313	7.0	–	CW	45.1	37.3	7.8			
I	CS	3.35	32.6	BoR	1160	0.2	82	WEAP	81.7	73.9	7.8	1.81	1.98	1.00
I	CT	3.35	32.6	EoID	1434	8.3	–	CW	42.6	37.4	5.2			
I	CT	3.35	32.6	BoR	1183	0.2	83	WEAP	82.2	77.0	5.2	1.93	2.06	1.00
I	CU	3.35	34.6	EoID	1149	8.2	–	CW	44.7	33.7	11.0			
I	CU	3.35	34.6	BoR	1096	0.2	52	WEAP	90.5	79.5	11.0	2.02	2.36	1.00
I	CV	3.35	34.6	EoID	1189	7.1	–	CW	47.6	36.2	11.4			
I	CV	3.35	34.6	BoR	1060	0.1	51	WEAP	91.0	79.6	11.4	1.91	2.20	1.00
J	DN	2.44	45.9	EoID	980	6.8	–	CW	42.2	36.5	5.7			
J	DN	2.44	45.9	BoR	945	3.0	0.5	CW	44.9	41.0	3.9	1.06	1.12	0.68

Notes: 1) CW indicates CAPWAP signal matching, IM indicates IMPACT signal matching and WEAP indicates GRLWEAP calibrated wave equation analyses;
2) Calibrated wave equation approach was used for sets < 2.5 mm. Selected results were also confirmed with IMPACT.

Table A2
Case studies – results.

Project	Pile Ref.	D (m)	L (m)	Case: EoID, BoR, static	Time (days)	Analysis type	R_{total} (MN)	R_{shaft} (MN)	R_{toe} (MN)	Setup		
										R_{total} (-)	R_{shaft} (-)	R_{toe} (-)
EURIPIDES	Loc1BN10	0.76	30.6	EoID	–	IM	4.7	2.2	2.5	–	–	–
EURIPIDES	Loc1CP1	0.76	30.5	Static, comp	7	–	7.9	4.0	3.9	1.68	1.82	1.56
EURIPIDES	Loc1BN3001	0.76	45.9	EoID	–	IM	13.1	10.1	3.0	–	–	–
EURIPIDES	Loc1CP2	0.76	47.0	Static, comp	12	–	18.2	14.3	3.9	1.39	1.42	1.30
EURIPIDES	Loc2BN3315	0.76	46.2	EoID		IM	13.9	10.9	3.0			
EURIPIDES	Loc2CP1	0.76	46.7	Static, comp	6		17.9	14.0	3.9	1.29	1.28	1.30
EURIPIDES	Loc2CP2	0.76	46.9	Static, comp	533	–	33.5	29.6	3.9	2.41	2.72	1.30
Horstwalde	1B	0.71	17.6	EoD	–	IM	1.92	1.74	0.17	–	–	–

(*continued on next page*)

Table A2 (*continued*)

Project	Pile Ref.	D (m)	L (m)	Case: EoID, BoR, static	Time (days)	Analysis type	R_{total} (MN)	R_{shaft} (MN)	R_{toe} (MN)	Setup		
										R_{total} (-)	R_{shaft} (-)	R_{toe} (-)
Horstwalde	1B	0.71	17.6	BoR	546	IM	4.28	4.11	0.17	2.23	2.36	1.00
Horstwalde	4D	0.71	17.7	EoD	–	IM	2.07	1.81	0.26	–	–	–
Horstwalde	4D	0.71	17.7	BoR	30	IM	3.42	3.25	0.18	1.65	1.79	0.67
TTB	T	2.00	30.6	EoID	–	CW	11.2	8.8	2.4			
TTB	T	2.00	30.6	Static, comp	52	–	32.4	26.1	6.2	2.89	2.99	2.56
TTB	P8	1.60	27.0	EoID	–	CW	8.5	8.2	0.3			
TTB	P8	1.60	27.0	Static, comp	75	–	24.0	19.1	4.9	2.82	2.33	–

References

Alm, T., Hamre, L., 2001. Soil model for pile driveability predictions based on CPT interpretations. In: Proceedings of the 15th Int. Conf. on Soil Mechanics and Foundation Engineering, Istanbul, Turkey, Pub. CRC Press, London, 1297-1302.

Argiolas, R., Jardine, R.J., 2017. An integrated pile foundation reassessment to support life extension and new build activities for a mature North Sea oil field project. In: Proceedings of the 8th Int. Conf. on Offshore Site Investigations and Geotechnics, Society for Underwater Technology, London. Vol. 2, 695-702.

Axelsson, G., 2000. Long-Term Set-Up of Driven Piles in Sand. Royal Institute of Technology, Stockholm, Sweden, PhD Thesis.

Baldi, G., Bellotti, R., Ghionna, V.N., Jamiolkowski, M., Lo Presti, D.C., 1989. Modulus of sands from CPTs and DMTs. In: Proceedings of 12th Int. Conf. on Soil Mechanics and Foundation Engineering, Rio de Janeiro. Balkema, Rotterdam, 165-170.

Barbosa, P., Geduhn, M., Jardine, R., Schroeder, F., Horn, M., 2015. Full scale offshore verification of axial pile design in chalk. In: Proceedings of the 3rd International Symposium Frontiers in Offshore Geotechnics (ISFOG), CRC Press, London, Vol. 1, 515-520.

Battacharya, S., Carrington, T., Aldridge, T., 2009. Observed increases in offshore pile driving response. Proceedings Geotechnical Engineering. ICE, London, pp. 71–80.

Bhushan, K., 2004. Design & installation of large diameter pipe piles for LAXT wharf. In: Proceedings Conference in Honor of George G. Gobel, Los Angeles, Americal Society of Civil Engineers, ASCE Geo-institute Reston, VA, USA, 370-389. https://doi.org/10.1061/40743(142)21

Buckley, R.M., Jardine, R.J., Kontoe, S., Barbosa, P., Schroeder, F.C., 2020. Full-scale observations of dynamic and static axial responses of offshore piles driven in chalk and tills. Géotechnique 70 (8), 657–681. https://doi.org/10.1680/jgeot.19.TI.001.

Bundesanstalt für Materialforschung und -prüfung (BAM), 2014. Experimenteller Tragfähigkeitsnachweis und Qualitätssicherung von Pfahlgründungen für Offshore Windkraftanlagen: Abschlussbericht zum Forschungsverbundprojekt. Fachbereich 7.2, Ingenieurbau, Berlin https://doi.org/10.2314/GBV:877878838 (in German).

Byrne, T., Doherty, P., Gavin, K., Overy, R., 2012. Comparison of Pile Driveability Methods in North Sea Sand. In: Proceedings of the 7th International Conference on Offshore Site Investigations and Geotechnics, Pub. Society for Underwater Technology, London, 481-488.

Carroll, R., Carotenuto, P., Dano, C., Salama, I., Silva, M., Rimoy, S., Gavin, K., Jardine, R.J., 2020. Field experiments at three sites to investigate the effects of age on steel piles driven in sand. Géotechnique 70 (6), 469–489. https://doi.org/10.1680/jgeot.17.P.185.

Cathie, D., Jaeck, C., Ozsu, E., Raymackers, S., 2020. Insights into the driveability of large diameter piles. In: Proceedings of the 4th Int. Symposium on Frontiers in Offshore Geotechnics, Austin, Texas. Ed: Z. Westgate, Pub. Deep Foundations Institute, Hawthorne New Jersey, USA, 757-766.

Cathie, D., Jardine, R. J., Silvano, R., Kontoe, S., Schroeder. F, 2022. Pile setup in sand – the "PAGE" joint industry project. Keynote paper. In: Proceedings of the 11th International Conference on Stress Wave Theory and Design and Testing Methods for Deep Foundations. Rotterdam. Sept 2022. Pub. KVI, The Hague, The Netherlands. https://zenodo.org/record/7148625#.Y9eN7HbP2Ul

Chow, F.C., 1997. Investigations into the behaviour of displacement pile for offshore foundations. Imperial College London (PhD thesis).

Deeks, A.J., Randolph, M.F., 1995. A simple model for inelastic footing response to transient loading. Int. J. Numer. Anal. Meth. Geomech. 19, 307–329. https://doi.org/10.1002/nag.1610190502.

Deutsche Gesellschaft für Geotechnik (DGGT), 2013. Recommendation on Piling (EA-Pfähle). Ernst & Sohn, Berlin.

DIN 18088-4, 2019. Structures for wind turbines and platforms – Part 4: Soil and foundation elements. Pub. Deutsches Institut Fur Normung, Berlin, Germany.

EC7, 2004. Eurocode 7: Geotechnical Design – Part 1: General rules, EN 1997–1:2004. Pub. CEN - European Committee for Standardisation, Brussels, Belgium.

Fellenius, B.H., 1988. Variation of CAPWAP results as a function of the operator. In: Proceedings of the 3rd Int. Conference on the Application of Stress-Wave Theory to Piles, Ottawa, Ed. B. Fellenius, Pub. BiTech Publishers, Vancouver, Canada, 814-825.

Galvis-Castro, A., Torvar-Valencia, R.D., Salgado, R., Prezzi, M., 2019. Effect of loading direction on the shaft resistance of jacked piles in dense sand. Géotechnique 69 (1), 16–28. https://doi.org/10.1680/jgeot.17.P.046.

Gavin, K., Jardine, R.J., Karlsrud, K., Lehane, B., 2015. The effects of pile ageing on the shaft capacity of offshore piles in sand. Keynote paper. In: Proceedings of the 3rd International Symposium Frontiers in Offshore Geotechnics (ISFOG), Oslo. CRC Press, London, Vol. 1, 129-152.

Gavin, K.G., Igoe, D.J.P., Kirwan, L., 2013. The effect of ageing on the axial capacity of piles in sand. Proc. Geotech. Eng. ICE, London 166 (2), 122–130. https://doi.org/10.1680/geng.12.00064.

Ho, Y.K., Jardine, R.J., Anh-Minh, N., 2011. Large displacement interface shear between steel and granular media. Géotechnique, 61 (3), 221-234. https://doi.org/10.1680/geot.8.P.086.

Jardine, R.J., 2020. Geotechnics, energy and climate change: the 56th Rankine Lecture. Géotechnique 70 (1), 3–59. https://doi.org/10.1680/jgeot.18.RL.001.

Jardine, R.J., Chow, F.C., 1996. New Design Methods for Offshore Piles. Pub, Marine Technology Directorate, London.

Jardine, R., Chow, F., Overy, R., Standing, J., 2005. ICP design methods for driven piles in sands and clays. Thomas Telford, London.

Jardine, R., Thomsen, N., Mygind, M., Thilsted, C.L., 2015. Axial capacity design practice for North European wind-turbine projects. In: Proceedings of the 3rd International Symposium Frontiers in Offshore Geotechnics (ISFOG), Oslo. CRC Press, London, Vol. 1, 581-592.

Jardine, R.J., Standing, J.R., Chow, F.C., 2006. Some observations of the effects of time on the capacity of piles driven in sand. Géotechnique 56 (1), 227–244. https://doi.org/10.1680/geot.2006.56.4.227.

Karlsrud, K., Jensen, T.G., Lied, E.K.W., Nowacki, F., 2014. Significant ageing effects for axially loaded piles in sand and clay verified by new field load tests. In: Proceedings of the 46th Offshore Technology Conference, Houston, Texas, USA, 1–19.

Kirsch, F., von Bargen, M., 2012. Offshore Windpark Nordsee Ost – Sichere Grundung bei Wind und Welle. Proc. Baugrundtagung Mainz, Pub. Deutsche Gesellschaft für Geotechnik e. V. (German Geotechnical Society), www.baugrundtagung.com.

Kolk, H., Vergobbi, P., Baaijens, A., 2005. Results from axial load tests on pipe piles in very dense sands: the EURIPIDES JIP. In: Proceedings of the 1st International Symposium Frontiers in Offshore Geotechnics (ISFOG), Perth, Australia, CRC Press, London, Vol. 1, 661-667.

Lehane, B.M., Schneider, J.A., Xu, X., 2005. The UWA-05 method for prediction of axial capacity of driven piles in sand. In: Proceedings of the 1st International Symposium Frontiers in Offshore Geotechnics (ISFOG), Perth, Australia, CRC Press, London, Vol. 1, 683–689.

Lehane, B.M., Lim, J.K., Carotenuto, P., Nadim, F., Lacasse, S., Jardine, R., dan Dijk, B., 2017. Characteristics of Unified Databases for Driven Piles. In: Proceedings of the 8th Int Conf on Offshore Site Investigations and Geotechnics, Pub. Society for Underwater Technology, London, UK, 162-191.

Lehane, B., Liu, Z., Bittar, E., Nadim, F., Lacasse, S., Jardine, R.J., Carotenuto, P., Jeanjean, P., Rattley, M., Gavin, K., Haavik, J., Morgan, N., 2020. A new "unified" CPT-based axial pile capacity design method for driven piles in sand, in the Proceedings of the 4th Int. Symposium on Frontiers in Offshore Geotechnics, Austin, Texas. Ed: Z. Westgate, Pub. Deep Foundations Institute, Hawthorne New Jersey, USA, 462-477.

Likins, G., Rausche, F., 2004. Correlation of CAPWAP with Static Load tests. In: Proceedings of the 7th Int. Conf. on the Application of Stress-wave Theory to Piles, Petaling Jaya, Selangor, Malaysia, 381-386.

Likins, G., Rausche, F., Thendean, G., Svinkin, M., 1996. CAPWAP correlation studies. In: Proceedings of the 5th International Conference on the Application of Stress-wave Theory to Piles, Orlando, FL, Pub. University of Florida, 447–464.

Lings, M.L., Dietz, M.S., 2005. The Peak Strength of Sand-Steel Interfaces and the Role of Dilation. Soils and Foundations. 45 (6), 1–14. https://doi.org/10.3208/sandf.45.1.

Loukidis, D., Salgado, R., Abou-Jaoude, G., 2008. Assessment of axially loaded pile dynamic design methods and review of INDOT axially loaded pile design procedure. Federal Highway Administration, Washington, USA, Report FHWA/IN/JTRP-2008/6.

Ohsaki, Y., 1982. Corrosion of steel piles driven in soils. Soils and Foundations. 22 (3), 57–76.

Overy, R., 2007. The use of ICP design method for the foundations of nine platforms installed in the UK North Sea. In: Proceedings of the of Int. Conf. on Offshore Site Investigation and Geotechnics, Society for Underwater Technology, London, UK, 256-366.

Pile Dynamics Inc (PDI), 2006. CAPWAP-Case pile wave analysis program. Background Report. Pub, PDI, Cleveland, Ohio, USA.

Pile Dynamics Inc (PDI), 2010. GRLWEAP. Background report. Pub, PDI, Cleveland, Ohio, USA.

Pile Dynamics Inc (PDI), 2014. CAPWAP Help. Pub, PDI, Cleveland, Ohio, USA.

Randolph, M.F., 2008. IMPACT – Dynamic analysis of impact driving – User manual for version 4.2. University of Western Australia, Perth, Australia.

Randolph, M.F., Simons, H.A., 1986. An improved soil model for one-dimensional pile driving analysis, in Proceedings of the 3rd Int. Conf. on Numerical Methods in Offshore Piling. Nantes. Editions Technip, France, pp. 3–17.

Randolph, M.F., 1993. Analysis of stress-wave data from pile tests at Pentre and Tilbrook. Proceedings of Large-scale pile tests in clay. Ed J Clarke, Pub. Thomas Telford, London, 436-447.

Rausche, F., Nagy, M., Webster, S., Liang, L., 2009. CAPWAP and refined wave equation analyses for driveability predictions and capacity assessment of offshore pile installations, OMAE2009-80163, Proc 28th Int. Conf. on Ocean, Offshore and Arctic Engineering, Honolulu, Pub. ASME, New York, USA, 1-9.

Rausche, F., Moses, F., Goble, G.G., 1972. Soil resistance predictions from pile dynamics, ASCE. J. Soil Mechanics and Foundations Div. 98 (9), 418–439.

Rausche, F., Goble, G., Likins, G., 1985. Dynamic Determination of Pile Capacity. ASCE J. Geotech. Eng. 111 (3), 367–383. https://doi.org/10.1061/(ASCE)0733-9410(1985)111:3(367).

Rausche, F., Likins, G., Liang, L., Hussein, M., 2010. Static and dynamic models for CAPWAP signal matching. Proceedings Geoflorida 2010 Art of Foundation Engineering Practice Congress. West Palm Beach, American Society of Civil Engineers, Reston, VA, pp. 534–553. https://doi.org/10.1061/41093(372)27.

Rimoy, S., Silva, M., Jardine, R., Yang, Z.X., Zhu, B.T., Tsuha, C.H.C., 2015. Field and model investigations into the influence of age on axial capacity of displacement piles in silica sands. Géotechnique 65 (7), 576–589.

Rücker, W., Karabeliov, K., Cuellar, P., Baeßler, M., Georgi, S., 2013. Großversuche an Rammpfählen zur Ermittlung der Tragfähigkeit unter zyklischer Belastung und Standzeit. In German. Geotechnik, Pub. Ernst & Sohn, Berlin 36, 77–89.

Sawai H., Yoshida Y., Sakai, T., 1996. Determination of the bearing capacity of large diameter pile from the dynamic loading test. 5th Int. Conf. Application Stress-Wave Theory Piles, Ed. F. Barends, Pub. Routledge, London, 788–796.

Sawai, H. 1998. Dynamic measurement method of bearing capacity of large diameter steel pipe pile, PhD Thesis, Hachinohe Institute of Technology, Aomori, Japan (in Japanese).

Shioi, Y., Yoshida, O., Meta, T., Homma, M., 1992. Estimation of bearing capacity of steel pipe pile by static loading and stresswave theory (Trans-Tokyo Bay Highway). In: Proceedings of the 4th Int Conference on Application of stress-wave theory to piles, Ed. F. Barends, Pub. Routledge, London, 325–330.

Skov, R., Denver, H., 1988. Time-dependence of bearing capacity of piles. In: Proceedings of the 3rd Int Conference on Application of stress-wave theory to piles, Ottawa, Ed. B. Fellenius, Pub. BiTech Publishers, Vancouver, Canada, 25–27.

Wen, K., Kontoe, S., Jardine, R.J., Liu, T., Cathie, D., Silvano, R., Prearo, C., Wei, S., Schroeder, F.C., Po, S., 2023. Assessment of time effects on capacities of large-scale piles driven in dense sands. Canadian Geotech. J. 60 (7), 1015–1035. https://doi.org/10.1139/cgj-2022-0060.

Yang, Z.X., Jardine, R.J., Zhu, B.T., Foray, P., Tsuha, C.H.C., 2010. Sand grain crushing and interface shearing during displacement pile installation in sand. Géotechnique 60 (6), 469–482. https://doi.org/10.1680/geot.2010.60.6.469.

Yang, Z.X., Guo, W.B., Jardine, R.J., Chow, F., 2017. Design method reliability assessment from an extended database of axial load tests on piles driven in sand. Can. Geotech. J. 54 (1), 59–74. https://doi.org/10.1139/cgj-2015-0518.

Zuidberg, H., Vergobbi, P., 1996. EURIPIDES, load tests on large driven piles in dense silica sands. In: Proceedings of the Offshore Technology Conference. Houston, Texas, USA, OTC 7977, 193-206.